analytical chemistry

Article

pubs.acs.org/ac

On-Target Labeling of Intracellular Metabolites Combined with Chemical Mapping of Individual Hyphae Revealing Cytoplasmic Relocation of Isotopologues

Jie-Bi Hu, Yu-Chie Chen,* and Pawel L. Urban*

Department of Applied Chemistry, National Chiao Tung University, 1001 University Rd, Hsinchu, 300, Taiwan

Supporting Information

ABSTRACT: A microscale analytical platform integrating microbial cell culture, isotopic labeling, along with visual and mass spectrometric imaging with single-cell resolution has been developed and applied in the monitoring of cellular metabolism in fungal mycelium. The method implements open chips with a two-dimensional surface pattern composed of hydrophobic and hydrophilic zones. Two hydrophilic islands are used as medium reservoirs, while the hydrophobic area constitutes the support for the growing aerial hyphae, which do not have direct contact with the medium. The first island, containing $^{12}C_6$-glucose medium, was initially inoculated with the mycelium (*Neurospora crassa*), and following the initial incubation period, the hyphae progressed toward the second medium island, containing an isotopically labeled substrate ($^{13}C_6$-glucose). The ^{13}C atoms were gradually incorporated into cellular metabolites, which was revealed by MALDI-MS. The fate of the chitin-biosynthesis precursor, uridine diphosphate *N*-acetylglucosamine (UDP-GlcNAc), was monitored by recording mass spectra with characteristic isotopic patterns, which indicated the presence of various $^{12}C/^{13}C$ isotopologues. The method enabled mapping the ^{13}C-labeled UDP-GlcNAc in fungal mycelium and recording its redistribution in hyphae, directly on the chip.

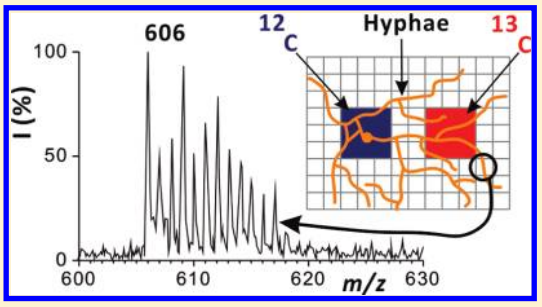

Fungi have been a human companion since the early days of civilization: they constitute an important part of the human diet, facilitate production of bread and alcoholic beverages, and produce useful bioactive compounds; however, they also diminish crops and affect human health.[1] Fungal mycelium represents primitive features of cell organization: more complex than unicellular organisms and simpler than one could encounter in animal or plant tissues. It is composed of hyphae, which enable long-distance transport of water, metabolites, nutrients, nuclei, and other micro- and nanoscopic species.[2] Due to their minuscule thickness (typically, 2−20 μm), it is challenging to study chemical processes (such as biosynthesis and transport of metabolites) occurring in individual hyphae. Numerous physiological phenomena take place on the single-cell level; however, only bulk samples of fungal mycelium, composed of many cells and hyphae, are usually subjected to biochemical analysis. The past few years have brought several key developments in the chemical imaging technology involving mass spectrometry (MS), two of which are matrix-assisted laser desorption/ionization (MALDI) and matrix-free laser desorption/ionization (LDI), techniques applicable to detection and mapping of biomolecules in tissue slices (for reviews, see refs 3−10), as well as compounds secreted by colonies of bacteria.[11−14] Technology also exists to enable mass spectrometric analysis and imaging of metabolites in single cells deposited on conductive supports (for reviews, see refs 15 and 16; examples of original work: refs 17−19). Isotopic labeling used in conjunction with mass spectrometry is a convenient way to reveal metabolic activity in single-cell specimens without absolute quantification.[20,21]

The goal of this study was to design and fabricate a microscale platform that would integrate the culture of fungal mycelium and isotopic labeling of intracellular metabolites, as well as optical and MS analysis of microscale specimens with single-cell resolution. The method enables observation of biosynthetic processes in fungal hyphae and cells and reveals relocation of the newly synthesized intracellular metabolites along the hyphae. The platform developed and used in this work implements open chips incorporating two-dimensional surface patterns composed of hydrophobic and hydrophilic zones (Figure 1). Two hydrophilic islands are used as reservoirs for ^{12}C- and ^{13}C-rich media, while the hydrophobic area constitutes the support for the growing aerial hyphae, which do not have direct contact with the medium. In addition, a grid was superimposed onto the surface in order to map the whole area of the chip and facilitate matching between optical and mass spectrometric images. When coupled with MALDI-MS, the platform allows one to observe the progress of metabolite labeling, as well as the relocation of metabolite isotopologues in fungal mycelium.

Received: April 4, 2012
Accepted: May 14, 2012
Published: May 14, 2012

dx.doi.org/10.1021/ac300903x | *Anal. Chem.* 2012, 84, 5110−5116

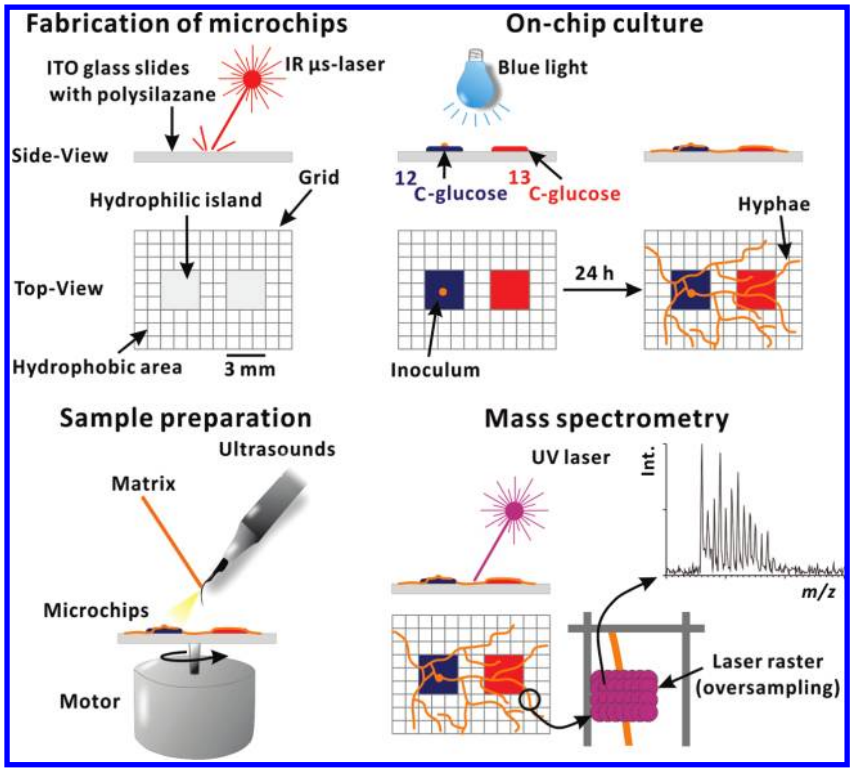

Figure 1. Development and application of the open microchip for mycelial culture, sequential isotopic labeling, and chemical mapping of individual hyphae.

EXPERIMENTAL SECTION

Fabrication of the Chips. In the first step, indium tin oxide (ITO)-glass slides were coated with a layer of polysilazane (for details of a related fabrication protocol, see, for example, ref 20). Microbiological medium recipients (3 × 3 mm), as well as the orientation grid, were created by ablation with an infrared (IR) μs-laser. The μs-laser engraving machine, SDPL-50W (Sintec Optronics Pte, Singapore), is equipped with a Nd:YAG DPSS laser (λ = 1064 nm) and controlled by the Laser Marker software (version 3.2.3.5; Jinan DuoWei Laser Technology, Jinan, Shandong, China). The following parameters were used: laser frequency, 2000 Hz; pulse width, 8 μs; hatch gap, 0.01 μm (double lines). After ablation, the microchip was cleaned with ethanol and water and dried. The hydrophilic islands were loaded with Vogel's medium containing 1.5% glucose as the only carbon source ($^{12}C_6$-glucose or $^{13}C_6$-glucose) and sterilized with ultraviolet (UV) light.

On-Chip Culture. A specimen containing conidia of *Neurospora crassa* strain (FGSC 988; Bioresource Collection and Research Center, Hsinchu, Taiwan) was used to inoculate the medium island containing 1.5% $^{12}C_6$-glucose (as a component of a modified Vogel's medium), Figure 1. The microchip was kept in the sterile conditions in a Petri dish containing a large droplet of water to maintain high humidity and to ensure that the medium held within the hydrophilic islands did not dry. The culture was illuminated with blue light (from an LED lamp; ~11 000 lux) for 16 h per 24-h cycle. In several hours, the hyphae grew outside the $^{12}C_6$-glucose medium island and progressed along the surrounding hydrophobic area. Some of the hyphae encountered the second medium island, which contained the medium with an isotopically labeled substrate, $^{13}C_6$-glucose, which was the only carbon source. From then on, the heavy carbon atoms were gradually incorporated into the molecules of metabolites in the mycelium.

As a side note, *Neurospora* is a filamentous ascomycete fungus. For over 70 years, it has served as one of the model eukaryotic organisms in molecular biology, and its genome has been sequenced.[22] It is easy to culture and manipulate, and it exhibits fast growth rates.

Preparation of Samples. First, individual hyphae were imaged by fluorescence microscopy (to gain information on the 2D structure of the hyphae, locations of branching sites, and the borderlines between cells). Second, cellular metabolism was quenched by coating the chip with a chemical matrix (3 mg mL^{-1} 9-aminoacridine in hexane/acetone 1:2 (v/v)) sprayed with an ultrasonic (kHz range) device. Third, following the displacement (extraction) of the ^{13}C-labeled metabolites from the hyphae to the adjacent area, an MS scan was executed (see Mass Spectrometry section).

The matrix coating method involved continuous-operation ultrasonic spray, as described elsewhere.[19] It enables gentle extraction of intracellular metabolites with moderate dispersion to the surrounding area. We used 9-aminoacridine (3 mg mL^{-1}, hexane/acetone 1:2 (v/v)) as the MALDI matrix. The flow rate of the matrix cocktail was 50 μL min^{-1}, and the deposition time was 30 min. In the current setup, a miniature electric motor was used to rotate the microchip during the application of the matrix, which facilitated homogeneous coating of the aerial hyphae leaning on the hydrophobic polysilazane-coated area of the chip.

Mass Spectrometry. All the MS measurements and imaging were conducted by means of the Autoflex III Smartbeam MALDI-MS instrument (Bruker Daltonics, Bremen, Germany), equipped with a solid-state laser (λ = 355 nm), and operated in the reflectron negative-ion mode. In the case of the high-resolution (single-cell) MS imaging, the laser beam

dx.doi.org/10.1021/ac300903x | *Anal. Chem.* 2012, 84, 5110−5116

was focused to a 10 μm spot, and the default spacing of the scan raster was set to 5 μm (oversampling); 100 laser shots were fired at each raster point with the preset frequency of 100 Hz. The mass range was normally set to 400−1000 Da, and all the ions up to 400 Da were excluded. Metabolite standards spotted on the side of the chip were used for mass calibration prior to the MS imaging. Metabolites present in *N. crassa* were identified by matching the observed m/z values with the predicted ones, as well as using tandem MS (cf. ref 23), and by taking into account the knowledge of which type of metabolites can be ionized using the 9-aminoacridine matrix (cf. ref 24).

Extraction of Metabolites from the Mycelium. In a control experiment, metabolites were extracted from the biomass of *N. crassa* grown in liquid medium. A small amount of mycelium (~200 mg) was harvested from the culture flask, mixed with acetonitrile, vortexed for ~1 h, and centrifuged (8000 rpm, 10 min). An aliquot of 1 μL of the resulting supernatant was then deposited onto the ground steel plate, mixed with 1 μL of the matrix solution (9 mg mL^{-1} 9-aminoacridine in acetone), and analyzed by MALDI-MS. In this way, we were able to record high-intensity signals from a number of fungal metabolites within the m/z range of interest (400−650).

RESULTS AND DISCUSSION

On-Chip Labeling. Using 9-aminoacridine as matrix, signals of several primary metabolites could be recorded in the MALDI mass spectra of *Neurospora crassa*. Figure 2 shows a

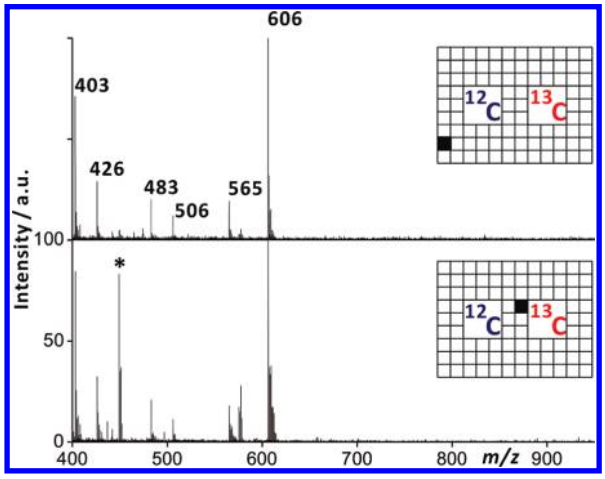

Figure 2. Broad m/z range MALDI mass spectra obtained at two different locations on the chip (cf. Figure 1) ~24 h after the inoculation of the $^{12}C_6$-glucose island with *Neurospora crassa*. Sampling positions and their orientation against the $^{12}C_6$- and $^{13}C_6$-glucose islands are indicated in the insets. At each location, 100 laser shots were fired. Peak assignment: m/z 403, uridine diphosphate; m/z 426, adenosine diphosphate; m/z 483, uridine triphosphate; m/z 506, adenosine triphosphate; m/z 565, uridine diphosphate glucose; m/z 606, uridine diphosphate *N*-acetylglucosamine. The peak marked with asterisk (*) is an unknown contaminant.

typical result obtained using the on-chip culture/biolabeling protocol outlined in Figure 1. When the hyphae cross and penetrate the $^{13}C_6$-glucose island, the ^{13}C atoms begin to be incorporated into the main metabolic pathways (glycolysis, TCA cycle, and others) and are built into metabolites; this can be judged on the basis of the emergence of isotopologue peaks next to the main metabolite peaks (Figure 2: top vs bottom).

We further focused on the spectral patterns of uridine diphosphate *N*-acetylglucosamine (UDP-GlcNAc), an important intermediate in biosynthesis of chitin, which can be recorded in the m/z range of 606−623. As observed in the low-resolution MALDI-MS images showing ion abundances while rasterring UV laser beam over the whole area of the chip ~48 h after the inoculation (Figure 3), relative abundances of UDP-

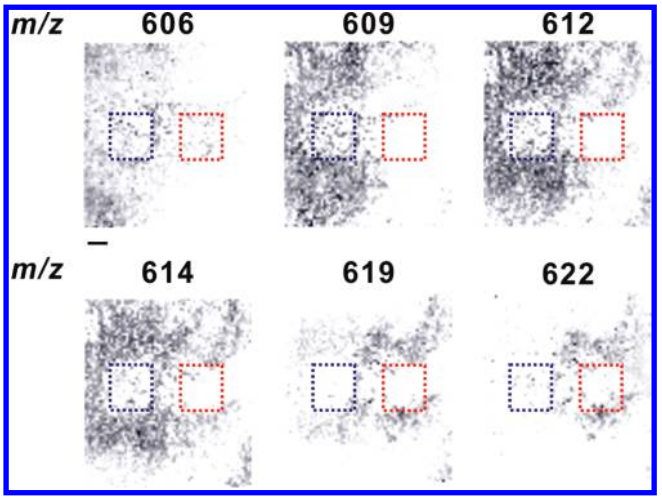

Figure 3. Low-resolution MALDI-MS images revealing zonal isotopic labeling of UDP-GlcNAc in the aerial mycelium of *Neurospora crassa* leaning on the chip (cf. Figure 1). The images were obtained ~48 h after the inoculation of the $^{12}C_6$-glucose island. Blue-color dotted line delimits the area loaded with $^{12}C_6$-glucose medium, while red-color dotted line delimits the area loaded with $^{13}C_6$-glucose medium. This result was obtained in a different experiment than the one depicted in Figure 2. Laser spot diameter: 90−100 μm; laser raster spacing: 200 μm. Scale bar: 1 mm.

GlcNAc molecules containing large numbers of ^{13}C atoms were higher in the proximity of the $^{13}C_6$-glucose island than near the $^{12}C_6$-glucose island (note the high abundance of $^{12}C_{11}{}^{13}C_6$−UDP-GlcNAc, m/z 612, near the $^{12}C_6$-glucose island, and the high abundance of $^{12}C_1{}^{13}C_{16}$−UDP-GlcNAc, m/z 622, near the $^{13}C_6$-glucose island).

In the next experiment, in order to map UDP-GlcNAc isotopologues within individual hyphae, we increased lateral resolution of the MALDI-MS scans (Figure 4A): the laser spot diameter was set to 10 μm, and the laser raster spacing was 5 μm. The mass spectrum corresponding to the region III (close to the $^{13}C_6$-glucose island) shows numerous isotopologues of UDP-GlcNAc (Figure 4A-right), while the mass spectrum corresponding to the region I (close to the $^{12}C_6$-glucose island) represents one high-intensity signal at the m/z 606 ($^{12}C_{17}{}^{13}C_0$ form of UDP-GlcNAc; Figure 4A-left). The spectrum collected in the zone between the $^{12}C_6$- and $^{13}C_6$-glucose islands (II) represents a partly labeled pool of UDP-GlcNAc molecules (Figure 4A-middle), where the labeling yield is less than in the region close to the $^{13}C_6$-glucose island (III). In this case, the intensity ratio calculated for the peaks at the m/z 607/606 is estimated to be ~41% (II); higher than that representative of the zone close to the $^{12}C_6$-glucose island: ~28% (I). On the basis of a simulation of the isotopic pattern using the Compass Isotope Pattern software (Bruker Daltonics), the intensity ratio at the m/z 607/606 for a nonlabeled UDP-GlcNAc is estimated to be ~20%. Therefore, this result indicates the relocation of the ^{13}C-label to more remote zones of the chip, which are

dx.doi.org/10.1021/ac300903x | *Anal. Chem.* 2012, 84, 5110−5116

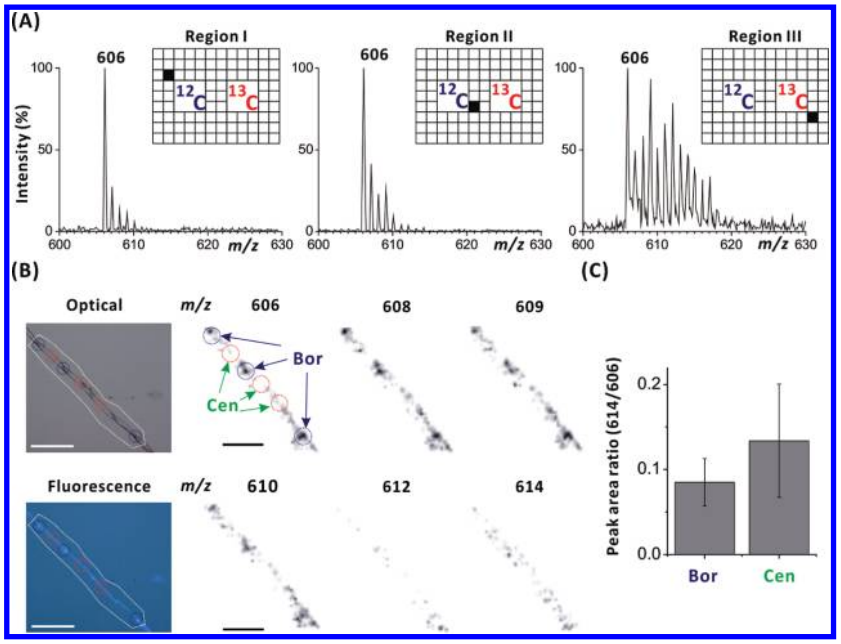

Figure 4. On-chip isotopic labeling, optical, and mass spectrometric imaging (cf. Figure 1). (A) Mass spectra obtained from individual hyphae in three different locations on the chip, labeled as regions I, II, and III (narrow m/z range revealing isotopic patterns of UDP-GlcNAc). Sampling positions and their orientation against the $^{12}C_6$- and $^{13}C_6$-glucose islands are indicated in the insets. Sampling time: ~24 h after the inoculation of the $^{12}C_6$-glucose island. (B) Optical, fluorescence (λ_{ex} = 330−380 nm), and MALDI-MS images (UDP-GlcNAc) of a hypha growing in the region III of the chip, i.e., close to the site containing $^{13}C_6$-glucose medium. Dark areas in the MS images indicate zones with a high signal intensity. Laser spot diameter: 10 μm; laser raster spacing: 5 μm. (C) Ratios of MS peak areas corresponding to a partly labeled (m/z 614) and the nonlabeled (m/z 606) form of UDP-GlcNAc recorded at different locations of the imaged hypha: Bor, at the cell borders (n = 64); Cen, in the central part of cells (n = 50; cf. blue and red color circles in (B) approximately mark the sampling positions). Error bars in (C) represent standard deviation. Since the data points in Bor and Cen do not represent normal distribution, we used a two-sample Kolmogorov−Smirnov test to compare the distributions of the values in these two data vectors (p < 0.01). These results were obtained in a different experiment than the ones depicted in Figures 2 and 3. Scale bars: 100 μm.

devoid of the growth medium and which are located a few millimeters away from the $^{13}C_6$-glucose island.

Since the protocol enables recording snapshots of metabolite profiles as a function of distance from the carbon source, it can facilitate following the fate of metabolites in dispersed biological systems, such as mycelial networks, without the need for the use of radioactive tracers. In fact, unlike in autoradiography-aided protocols,[25] the use of imaging mass spectrometry allowed us to monitor selected metabolites, as well as their isotopologues, while still maintaining single-hypha resolution. An alternative protocol, based on secondary ion mass spectrometry, can provide distribution of low-molecular-weight fragment ions of isotopically labeled metabolites with high lateral resolution;[21] conversely, the present method enables mapping intact metabolite isotopologues in individual cells. While a previous study demonstrated single-cell analysis of yeast labeled with carbon-13 before the application of the cell suspension to a MALDI target,[20] here we demonstrate the isotopic labeling which takes place directly on the target. This can simplify the experiment, decrease the bias related to the sample preparation step, and gain new insight to biosynthesis of cellular metabolites. Overall, the chips used in this study are compatible with cell culture, isotopic labeling, metabolite extraction, and the analysis by MS. The design of the chip addresses the characteristics of fungal growth (at the interface of solid substrate and ambient air) and enables ionization of metabolites with the beam of ultraviolet (UV) laser light in the vacuum compartment of a mass spectrometer.

Single-Cell Imaging. Due to the fact the chips are transparent, the cultured specimens could be visualized with optical and fluorescence microscopy prior to the MS analysis/imaging: this enabled identification of the microscopic features within the hyphae, for example, borderlines between the cells located along hyphae. The thin grid lines (created by the ablation with the IR μs-laser) were used to locate the hyphal regions, which were sequentially imaged by optical/fluorescence microscopy and MS (Figure 4B). The MS images obtained for a single hypha growing in the region III of the chip (near the $^{13}C_6$-glucose island) reveal the distributions of the nonlabeled ($^{12}C_{17}{}^{13}C_0$) and various labeled ($^{12}C_{\leq 16}{}^{13}C_{\geq 1}$) forms of UDP-GlcNAc. The comparison of the optical/fluorescence and MS micrographs suggests that a higher level of UDP-GlcNAc occurs at the cell borders than in the central part of each cell (Figure 4B). In addition, we found that the ratio of a partly labeled ($^{12}C_9{}^{13}C_8$) and the nonlabeled ($^{12}C_{17}{}^{13}C_0$) forms of UDP-GlcNAc is higher near the cell centers than at the cell borders (Figure 4C). On the basis of the result of a nonparametric statistical test, the peak area ratio (m/z 614/606) values determined for the cell border (Bor) and the cell center (Cen) regions are from different continuous distributions.

Obtaining good-quality MS images of single cells/hyphae relies on careful application of the matrix cocktail; thus, a number of matrix deposition strategies have been developed (e.g., refs 26−29). Too fast of a matrix deposition wets the sample, invites dispersion of metabolites, and leads to blurred MS images, in which microscopic features of chemical gradients cannot be observed on the single-cell level. Therefore, the speed of the matrix deposition using the ultrasonic spray had to be tuned in a series of preliminary experiments; eventually, we

dx.doi.org/10.1021/ac300903x | Anal. Chem. 2012, 84, 5110−5116

chose the flow rate of 50 μL min^{-1}. Further on, in order to obtain lateral resolution sufficient for mapping the contents of single hyphae, here we applied the "oversampling" scan method (adjacent positions of the laser scan are overlapped)[30] together with a 10 μm beam of UV laser light. Such a combination of scan parameters provided sufficient lateral resolution to observe distribution of metabolites along hyphae (Figure 4B). Spatial separation of the hydrophilic islands containing the growth medium ($^{12}C_6$- or $^{13}C_6$-glucose) and the surrounding hydrophobic area, that supports progression of aerial hyphae, serves two main purposes: First, movements of carbon isotopes (^{12}C, forward, and ^{13}C, backward) can unambiguously be judged upon the relative peak intensities of metabolite isotopologues in relation to the sampling position on the chip. Second, since only the hyphae present outside the medium islands of the open chip are analyzed by MS, there is no ion suppression effect due to the presence of agar medium. In addition, the thin nature of hyphae allowed us to circumvent the possible ion-suppression effect in the imaged sections. It should be noted that spatial resolution might further be enhanced using state-of-the-art MS instrumentation using thinner ($\leq$5 μm) laser beams, similar to the one described by Römpp et al.[31]

Control Experiments. In order to verify the possibility of labeling fungal mycelium on the proposed open chip platform, further control experiments were carried out without preservation of single-hypha resolution. Figure 5 shows progressive labeling of UDP-GlcNAc in *N. crassa* cultured on the chip according to the protocol outlined in Figure 1: unlike in Figure 4, the spectra were acquired for multiple hyphae in order to obtain higher signal-to-noise ratios. A comparison of mass spectra obtained 24 and 48 h (Figure 5A,B, respectively) after the inoculation of the $^{12}C_6$-glucose island suggests that the greatest amount of carbon-13 got incorporated by the mycelium between 24 and 48 h. A nonspecific labeling pattern can be observed for UDP-GlcNAc monitored 48 h after the inoculation (Figure 5B).

In another control experiment, the mycelium of *N. crassa* was transferred to a liquid medium containing $^{13}C_6$-glucose as the only carbon source (cf. Experimental Section). Subsequent analysis of the extracts from mycelium by MALDI-MS (Figures 6A,B) and MALDI-MS/MS (Figure 6C,D) revealed the progress of labeling of the cellular metabolites, including UDP-GlcNAc. Compared with the nonlabeled mycelium (Figure 6A), the relative abundance of the UDP-GlcNAc with 8 ^{13}C atoms (m/z 614) significantly increased over 12 h, while lighter and heavier forms of the same metabolite were less abundant (Figure 6B). Following an 18-h incubation with $^{13}C_6$-glucose medium, relative abundances of the isotopologues with 0, 8, 16, and 17 ^{13}C atoms (m/z 606, 614, 622, and 623) were comparable. After 48 h, heavy forms of the metabolite (m/z 622 and 623) dominated the spectrum, and the nonlabeled form (m/z 606) was not detectable. The occurrence of spectral regions with high (m/z 614, 619–623) and low (m/z 607–613, 615–618) intensities (Figure 6B) suggests sequential labeling of the UDP-GlcNAc pool during the culture in liquid medium and the existence of fast and slow biosynthetic steps. In order to verify this assumption, we conducted MS/MS analysis of the nonlabeled (m/z 606) and partly labeled (m/z 614) ions used as parent ions in the postsource-decay fragmentation process aided with the laser-induced fragmentation technology (LIFT) (Figure 6C): On the basis of the shift of the peak at the m/z 282 to the m/z 290 (and m/z 362 to 370) and no significant shift of the fragment ion peak at the m/z 385, we conclude that

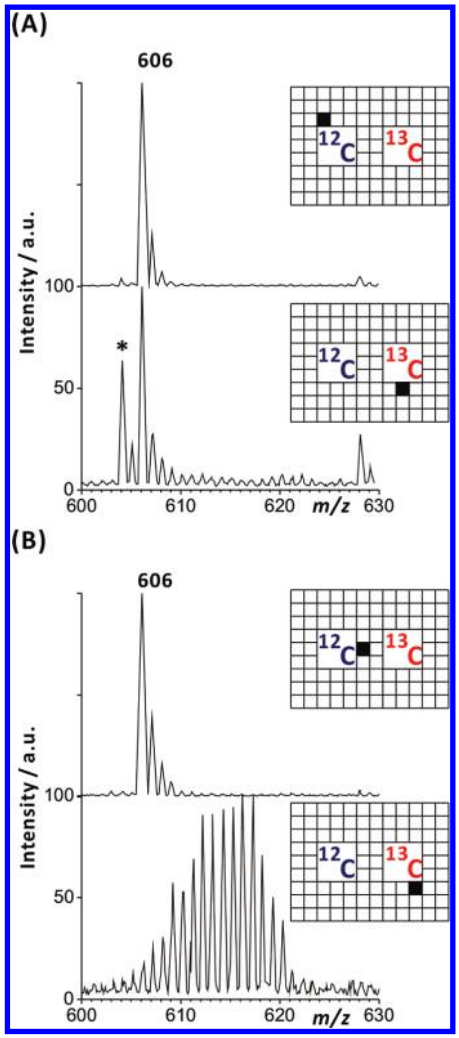

Figure 5. Progressive labeling of UDP-GlcNAc in *Neurospora crassa* cultured on the chip according to the protocol outlined in Figure 1. Mass spectra obtained (A) 24 and (B) 48 h after the inoculation of the $^{12}C_6$-glucose island. The upper spectra in (A) and (B) were obtained at sampling sites near the $^{12}C_6$-glucose islands, while the lower spectra in (A) and (B) were obtained at sampling sites near the $^{13}C_6$-glucose islands. The exact sampling positions (indicated in the insets) were chosen on the basis of the presence/abundance of hyphae within the sampling squares around the medium islands. The peak at the m/z 606 is unlabeled UDP-GlcNAc; the peak marked with an asterisk (*) is an unknown compound. These results were obtained in a different experiment than the ones depicted in the previous figures; here the spectra were acquired for multiple hyphae.

the *N*-acetylglucosamine (GlcNAc) moiety has been labeled with ^{13}C before the labeling of the uridine disphosphate (UDP) moiety (Figure 6D), which is in agreement with a model of UDP-GlcNAc biosynthesis outlined in Figure S1, Supporting Information.

A comparison of the spectra collected in the proximity of the $^{13}C_6$-glucose island on the chip (Figure 5-lower panels) with the spectra obtained from the mycelium from the liquid culture (Figure 6B) clearly shows differences in the labeling patterns obtained with these two labeling approaches. This observation is explained in the following way: when the hyphae reach the $^{13}C_6$-glucose island, a large amount of biosynthetic precursors rich in carbon-12 has to be transported from the distant $^{12}C_6$-glucose island via cytosol, and few carbon-13 atoms obtained

dx.doi.org/10.1021/ac300903x | *Anal. Chem.* 2012, 84, 5110–5116

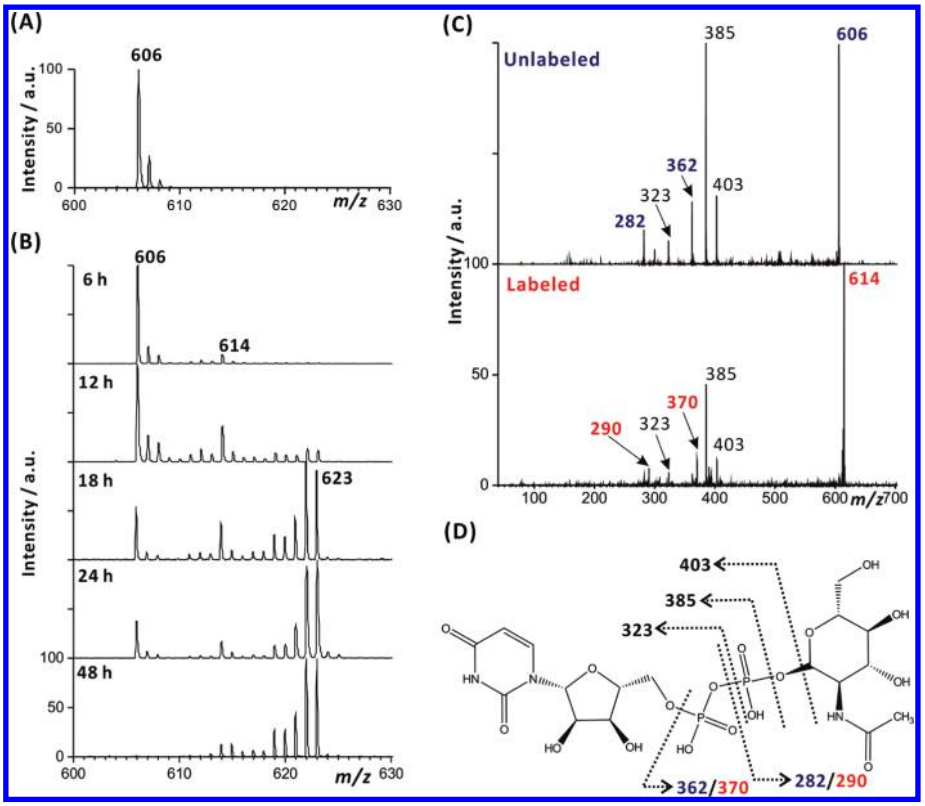

Figure 6. Progressive labeling of UDP-GlcNAc in *Neurospora crassa* cultured in liquid medium. Mycelium was obtained from a culture using $^{12}C_6$-glucose medium and further incubated with $^{13}C_6$-glucose medium. Analysis by MALDI-MS (A and B) and MALDI-MS/MS (C and D) in the negative-ion mode. (A) Mass spectrum of the mycelium incubated with $^{12}C_6$-glucose for ~48 h. (B) Mass spectrum of the mycelium incubated with $^{13}C_6$-glucose for 6–48 h. (C) Tandem mass spectra of the ions recorded at the *m*/*z* 606 and 614 (cf. B: ~12 h after the inoculation of the $^{13}C_6$-glucose medium). (D) Chemical structure of UDP-GlcNAc revealing the characteristic fragments observed in the tandem mass spectra in (C). Red-color font indicates the fragments labeled with carbon-13.

from the newly colonized $^{13}C_6$-glucose island are incorporated to the primary metabolic pathways (Figure S1, Supporting Information). Since the culture environment is nonhomogeneous (two islands with the $^{12}C_6$- and $^{13}C_6$-glucose media surrounded by the hydrophobic area without medium), mixing of $^{12}C_x{}^{13}C_y$ isotopologues of metabolic intermediates, transported by cytosol from cell to cell, occurs. Following a longer contact of hyphae with the $^{13}C_6$-glucose island, hyphal metabolism switches from vegetative growth in the nutrient-poor environment (hydrophobic area of the chip) to the exploration of the new carbon source ($^{13}C_6$-glucose). This can lead to a sudden increase in the amount of carbon-13 incorporated to UDP-GlcNAc molecules (Figure 5B). This labeling scheme is different than the one observed using liquid culture (Figure 6B), in which case $^{13}C_6$-glucose is easily available to all cells, and can immediately be incorporated into all metabolic pathways (Figure S1, Supporting Information). In the case of the chip-based protocol, the labeling is limited by the separation of ^{12}C and ^{13}C sources (two islands with the $^{12}C_6$- and $^{13}C_6$-glucose media). On the other hand, the labeling in the liquid culture is only limited by the rates and numbers of biosynthetic steps, which naturally leads to the formation of the characteristic labeling patterns observed in Figure 6B.

■ CONCLUSIONS

In summary, a chip integrating isotopic labeling of intracellular metabolites (as exemplified by UDP-GlcNAc), microbial cell culture, and mass spectrometric imaging at single-hypha resolution has been demonstrated. The compatibility of these three steps has been shown. The method allows one to map the biosynthesis of cellular metabolites and their redistribution in a multicellular system, such as fungal mycelium. The combination of the on-chip stable-isotope labeling and the MS imaging with single-cell resolution provides high chemical selectivity and sensitivity. It ensures control over the experimental parameters and enables in situ preparation of microscale samples, minimizing perturbation of the biological system. Despite the small size of the hyphae (width, ~10 μm), the signal intensity was sufficient to map high-abundance intracellular metabolites. Here we have tested the new method for its ability to assist the monitoring of cellular metabolism: the result revealed relocation of the isotopic labels along the hyphae. Although implementation of MALDI-MS as a readout technique may contribute to certain analytical biases (e.g., different ion yields for different compounds, sample matrix interference, "sweet spot" effect), here these drawbacks are decreased to some extent thanks to the usage of isotopic labels.

We think the proposed strategy may further be extended to the studies of metabolism in fungi and other species which exhibit simple organization of cells. Due to the separation of ^{12}C and ^{13}C carbon sources, the influence of the translocation of metabolic intermediates on biosynthetic processes in a multicellular system can be studied. In the future, it would be interesting to combine the proposed on-target labeling method with ambient MS ion sources, which would circumvent insertion of the biological specimens to the high-vacuum compartment of mass spectrometer. To this point, the lateral

dx.doi.org/10.1021/ac300903x | *Anal. Chem.* 2012, 84, 5110–5116

resolution of ambient MS imaging techniques needs to be improved to reach the low-micrometer (≤10 μm) level, to make the visualization of metabolite gradients in fungal hyphae possible.

■ ASSOCIATED CONTENT

Supporting Information

Additional information as noted in text. This material is available free of charge via the Internet at http://pubs.acs.org.

■ AUTHOR INFORMATION

Corresponding Author

*Fax: +886-3-5723764.

Notes

The authors declare no competing financial interest.

■ ACKNOWLEDGMENTS

We thank the National Science Council of Taiwan for the financial support of this work.

■ REFERENCES

(1) Kavaler, L. *Mushrooms, Molds, and Miracles*; The New American Library: New York, 1966.
(2) Read, N. D.; Lichius, A.; Shoji, J. Y.; Goryachev, A. B. *Curr. Opin. Microbiol.* **2009**, *12*, 608−615.
(3) Cornett, D. S.; Reyzer, M. L.; Chaurand, P.; Caprioli, R. M. *Nat. Methods* **2007**, *4*, 828−833.
(4) Reyzer, M. L.; Caprioli, R. M. *Curr. Opin. Chem. Biol.* **2007**, *11*, 29−35.
(5) Burnum, K. E.; Frappier, S. L.; Caprioli, R. M. *Annu. Rev. Anal. Chem.* **2008**, *1*, 689−705.
(6) Cornett, D. S.; Frappier, S. L.; Caprioli, R. M. *Anal. Chem.* **2008**, *80*, 5648−5653.
(7) Chughtai, K.; Heeren, R. M. A. *Chem. Rev.* **2010**, *110*, 3237−3277.
(8) Svatoš, A. *Trends Biotechnol.* **2010**, *28*, 425−434.
(9) Chaurand, P.; Cornett, D. S.; Angel, P. M.; Caprioli, R. M. *Mol. Cell. Proteomics* **2011**, *10*, 1−11.
(10) Vickerman, J. C. *Analyst* **2011**, *136*, 2199−2217.
(11) Esquenazi, E.; Yang, Y.-L.; Watrous, J.; Gerwick, W. H.; Dorrestein, P. C. *Nat. Prod. Rep.* **2009**, *26*, 1521−1534.
(12) Yang, Y. L.; Xu, Y.; Straight, P.; Dorrestein, P. C. *Nat. Chem. Biol.* **2009**, *5*, 885−888.
(13) Yang, Y.-L.; Xu, Y.; Kersten, R. D.; Liu, W.-T.; Meehan, M. J.; Moore, B. S.; Bandeira, N.; Dorrestein, P. C. *Angew. Chem., Int. Ed.* **2011**, *50*, 5839−5842.
(14) Phelan, V. V.; Liu, W.-T.; Pogliano, K.; Dorrestein, P. C. *Nat. Chem. Biol.* **2012**, *8*, 26−35.
(15) Rubakhin, S. S.; Romanova, E. V.; Nemes, P.; Sweedler, J. V. *Nat. Methods* **2011**, *8*, S20−S29.
(16) Svatoš, A. *Anal. Chem.* **2011**, *83*, 5037−5044.
(17) Rubakhin, S. S.; Greenough, W. T.; Sweedler, J. V. *Anal. Chem.* **2003**, *75*, 5374−5380.
(18) Hölscher, D.; Shroff, R.; Knop, K.; Gottschaldt, M.; Crecelius, A.; Schneider, B.; Heckel, D. G.; Schubert, U. S.; Svatoš, A. *Plant J.* **2009**, *60*, 907−918.
(19) Urban, P. L.; Chang, C. H.; Wu, J. T.; Chen, Y.-C. *Anal. Chem.* **2011**, *83*, 3918−3925.
(20) Urban, P. L.; Schmidt, A. M.; Fagerer, S. R.; Amantonico, A.; Ibañez, A.; Jefimovs, K.; Heinemann, M.; Zenobi, R. *Mol. BioSyst.* **2011**, *7*, 2837−2840.
(21) Steinhauser, M. L.; Bailey, A. P.; Senyo, S. E.; Guillermier, C.; Perlstein, T. S.; Gould, A. P.; Lee, R. T.; Lechene, C. P. *Nature* **2012**, *481*, 516−519.
(22) Galagan, J. E.; Calvo, S. E.; Borkovich, K. A.; et al. *Nature* **2003**, *422*, 859−868.
(23) Sun, G.; Yang, K.; Zhao, Z.; Guan, S.; Han, X.; Gross, R. W. *Anal. Chem.* **2007**, *79*, 6629−6640.
(24) Edwards, J. L.; Kennedy, R. T. *Anal. Chem.* **2005**, *77*, 2201−2209.
(25) Miguelez, E. M.; García, M.; Hardisson, C.; Manzanal, M. B. *J. Bacteriol.* **1994**, *176*, 2105−2107.
(26) Zimmerman, T. A.; Rubakhin, S. V.; Romanova, E. V.; Tucker, K. R.; Sweedler, J. V. *Anal. Chem.* **2009**, *81*, 9402−9409.
(27) Vrkoslav, V.; Muck, A.; Cvacka, J.; Svatoš, A. *J. Am. Soc. Mass Spectrom.* **2010**, *21*, 220−231.
(28) Yang, J.; Caprioli, R. M. *Anal. Chem.* **2011**, *83*, 5728−5734.
(29) Thomas, A.; Charbonneau, J. L.; Fournaise, E.; Chaurand, P. *Anal. Chem.* **2012**, *84*, 2048−2054.
(30) Jurchen, J. C.; Rubakhin, S. S.; Sweedler, J. V. *J. Am. Soc. Mass. Spectrom.* **2005**, *16*, 1654−1659.
(31) Römpp, A.; Guenther, S.; Schober, Y.; Schulz, O.; Takats, Z.; Kummer, W.; Spengler, B. *Angew. Chem., Int. Ed.* **2010**, *49*, 3834−3838.